Automated Blood Vessel Segmentation of Fundus Images Using Region Features of Vessels

Zhun Fan

Guangdong Provincial Key Laboratory of
Digital Signal and Image Processing,
Department of Electronic Engineering
Shantou University
Guangdong, Shantou 515063

Jiewei Lu

Department of Electronic Engineering
Shantou University
Guangdong, Shantou 515063

Yibiao Rong

Department of Electronic Engineering
Shantou University
Guangdong, Shantou 515063

Abstract—**This paper proposes a novel and simple unsupervised vessel segmentation algorithm using fundus images. At first, the green channel of a fundus image is preprocessed to extract a binary image after the isotropic undecimated wavelet transform, and another binary image from the morphologically reconstructed image. Secondly, two initial vessel images are extracted according to the vessel region features for the connected regions in binary images. Next, the regions common to both initial vessel images are extracted as the major vessels. Then all remaining pixels in two initial vessel images are processed with skeleton extraction and simple linear iterative clustering. Finally the major vessels are combined with the processed vessel pixels. The proposed algorithm outperforms its competitors when compared with other widely used unsupervised and supervised methods, which achieves a vessel segmentation accuracy of 95.8% and 95.8% in an average time of 9.7s and 14.6s on images from two public datasets DRIVE and STARE, respectively.**

I. INTRODUCTION

The morphological attributes of retinal blood vessels play an important role in diagnosis, treatment, and evaluation of various ophthalmologic diseases. Any damage to retinal vessels can result in acquired blindness. Vascular diseases are closely related to public health problem of society. Since the detection and analysis on fundus images is vital to many clinical applications, an accurate vessel segmentation algorithm with low computational complexity is desired for the vessel analysis system.

Broadly speaking, all of the established algorithms for automated blood vessels segmentation using fundus images can be divided into unsupervised and supervised algorithms. In terms of supervised algorithms, the trained classifiers such as neural network [1], k-nearest neighbor (kNN) [2], decision trees [3], and adaboost [4] have been applied to extract blood vessels from fundus images. In the unsupervised category of algorithms, a lot of effective algorithms such as line detectors [5], morphological transformations [6] or model-based methods [7] are used to label the pixels on fundus images as vessel or not. In this paper, a novel and simple vessel segmentation method is proposed that firstly segments the major vessels, and then adds processed vessel pixels by using skeleton extraction [8] and simple linear iterative clustering (SLIC) [9]. This simple approach performs well on fundus images, and has higher computational efficiency than most methods.

This paper proposes a novel and simple blood vessel segmentation method, where region features of blood vessels are applied to segment initial estimates of vasculature, and 7 region features of blood vessel are defined and utilized. These regions features are able to describe the shape of blood vessels and proved to be suitable in the detection and analysis of blood vessel. The proposed vessel segmentation algorithm require less segmentation time and achieves consistent vessel segmentation accuracy on normal images as well as images with pathology, uneven illumination, pigmentation and fields of view (FOV) when compared with other methods.

The remainder of the paper is structured as follows: Section II illustrates the proposed method and materials. In Section III, the experimental results are presented. Section IV gives a short discussion.

II. METHODS AND DATASETS

The proposed algorithm for vessel segmentation is performed as follows: Firstly, two binary images are obtained by thresholding two vessel enhanced images, one is preprocessed by isotropic undecimated wavelet transform (IUWT) [10] and another by morphological reconstruction [3]. Secondly, region features of blood vessels are used to extract initial segmented vessels. Next, the regions common to both initial segmented vessel images are extracted as the major vessels. At last, skeleton extraction and simple linear iterative clustering (SLIC) are used to process the rest of pixels in two initial vessel images. The proposed algorithm is evaluated on two public datasets.

A. Datasets

In order to evaluate the vessel segmentation algorithm, two publicly available datasets containing fundus images were used.

DRIVE [11] dataset includes 40 images with $45°$ FOV, obtained in the course of a diabetic retinopathy screening program in the Netherlands. This dataset is divided into a test set (DRIVE Test) and a training set (DRIVE Train) with 20 images respectively.

STARE [12] dataset includes 20 images with 35° FOV, captured by a TopCon TRV-50 fundus camera. This dataset includes ten normal images (STARE Normal) and ten abnormal images (STARE Abnormal).

B. Proposed Method

1) Vessel Enhancement: The green channel of a fundus image is regularized in $[0,1](I)$ firstly. Each image (I) is reversed to transform the vessel regions into the brightest regions, resulting in image (I_c). Then I_c is subjected to vessel enhancement followed by IUWT and morphological reconstruction.

IUWT: Before applying IUWT, firstly I_c is subjected to morphological top-hat transformation (disc structuring element of length 8 pixels in radius) with the purpose of removing vessel central light reflex [1], resulting in image I_t. Applied to a signal $c_0 = I_t$, subsequent scaling coefficients are calculated by convolution with a filter $h^{\uparrow j}$

$$c_{j+1} = c_j * h^{\uparrow j}$$

where $h_0 = [1,4,6,4,1]/16$ is derived form the cubic B-spline, $h^{\uparrow j}$ is the upsampled filter obtained by inserting $2^j - 1$ zeros between each pair of adjacent coefficients of h_0. Wavelet coefficients are the difference between two adjacent sets of scaling coefficients, i.e.,

$$w_{j+1} = c_j - c_{j+1}$$

After the computation of n wavelet levels

$$I_t = c_n + \sum_{j=1}^{n} w_j$$

In vessel segmentation, wavelet scales:2-3 are selected according to [10], thereby resulting in vessel enhanced image T_i.

Morphological reconstruction: The morphological top-hat reconstruction is listed in Equation (1),

$$I_{th}^\theta = I_c - (I_c \circ S_e^\theta) \qquad (1)$$

where "I_{th}^θ" is the top-hat reconstruction image, "S_e^θ" is structuring elements for morphological opening, "$\circ$", and "θ" is the angular rotation of the structuring element. The chosen structuring element is 1-pixel width and 21-pixels length. Its size fits the diameter of the biggest vessels approximately in the retinal images.

$$T_m = \sum_{\theta \in A} I_{th}^\theta \qquad (2)$$

The sum of top-hat reconstruction T_m is defined in Equation (2). Each angular orientation of structuring elements belongs to set "A", which can be defined as $\{x|0 < x < \pi \ \& \ x \bmod (\pi/12) = 0\}$. The sum of the top-hat reconstruction on the retinal image can enhance each vessel, resulting in a vessel enhanced image T_m.
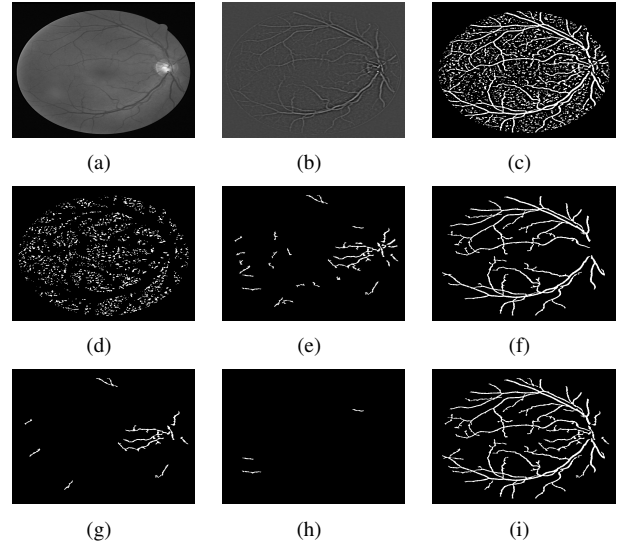

Fig. 1: Vessel segmentation after IUWT on an image from the DRIVE dataset. (a) Green plane image (I). (b)Vessel enhanced image (T_{i0}). (c)Threshold image (V_{i0}) (d)$V_{i1}(0 < Area_{V_{i0}}) < a_{i1}$). (e)$V_{i2}(a_{i1} \le Area_{V_{i0}} < a_{i2}$). (f)$V_{i3}(Area_{V_{i0}} \ge a_{i2})$. (g)$V_{i2a}(Extent_{V_{i2}} < e_{i1})$. (h)$V_{i2b}(Extent_{V_{i2}} > e_{i2}\&\&VBRatio_{V2} > r_i)$. (i)The final segmented vessels (VIF).

Algorithm 1 : Vessel Segmentation After IUWT

Input:
Vessel Enhanced Image T_{i0}
Output:
The final segmented vessel image (VIF)
Process:

$$\forall(x,y), \quad V_{i0}(x,y) = \begin{cases} 1 & if \ T_{i0}(x,y) > p_i \\ 0 & otherwise \end{cases}$$

$$V_{i0} = \begin{cases} V_{i1} & if \ 0 < Area_{V_{i0}} < a_{i1} \\ V_{i2} & if \ a_{i1} \leqslant Area_{V_{i0}} < a_{i2} \\ V_{i3} & if \ Area_{V_{i0}} \geqslant a_{i2} \end{cases}$$

Let $a = [a1_{V_{i2}}, a2_{V_{i2}}, a3_{V_{i2}}, ..., an_{V_{i2}}]$ represent labels of each connected regions in V_{i2}

$$\forall x \in a \quad V_{i2a} = \begin{cases} 1 & if \ Extent_x < e_{i1} \\ 0 & otherwise \end{cases}$$

$$V_{i2b} = \begin{cases} 1 & if \ Extent_x > e_{i2} \ \&\& \ VBRatio_x > r_i \\ 0 & otherwise \end{cases}$$

$$VIF = V_{i3} \cup V_{i2a} \cup V_{i2b}$$

---

2) Vessel Segmentation: Two binary images V_{i0} and V_{m0} are obtained by global thresholding the vessel enhanced image T_i and T_m for pixels greater than "p_i" and "p_m":$p_i \in [-0.2, 0.2]$, $p_m \in [0,1]$. For images from DRIVE and STARE datasets, optimal values of "$p_i = 0.003$" and "$p_m = 0.3$" are selected to retain the 4-connected regions [8] as much as possible and minimizing error in the final segmented vessel image.

For each 4-connected region in V_{i0} or V_{m0}, 7 effective region features of blood vessels are defined and used to classify it as vessel region or not.

- **Area** is the number of pixels in each connected region.

- **Bounding Box** specifies the smallest rectangle containing the connected region.
- **Extent** is the proportion of pixels in the connected region to pixels in the total bounding box. *Extent* reflects the extensibility of each connected region. Generally blood vessel performs well on extensibility.
- **VBRatio** is the ratio of width and length of bounding box and used to describe the shape of blood vessels. The value of *VRation* of vessels is larger than nonvessels in general.
- **ConvexArea** specifies the number of pixels in convex hull. Convex Hull specifies the smallest convex polygon that can contain the connected region.
- **Solidity** is the ratio of the pixels in the convex hull that are also in the region and is computed as *Area/ConvexArea*. It is used to describe the solidity of each connected region.
- **VCRatio** is the ratio of *Extent* and *Solidity*. It reflects the comprehensive situation of extensibility and solidity of blood vessels.

For binary image V_{i0}, at first, the 4-connected regions in V_{i0} are divided into three parts according to *Area* of each connected region: $V_{i1}(0 < Area_{V_{i0}} < a_{i1})$, $V_{i2}(a_{i1} \le Area_{V_{i0}} < a_{i2})$ and $V_{i3}(Area_{V_{i0}} \ge a_{i2})$. V_{i3} is preserved while V_{i1} is abandoned since almost all connected regions in V_{i3} appear as vessel regions, but most of connected regions in V_{i1} belong to noise region. Secondly, we retain the connected regions in V_{i2} whose $Extent_{V_{i2}}$ is less than e_{i1} since it is more likely that the region having high extended level belongs to vessel regions (V_{i2a}). At Last, the connected regions in V_{i2} whose $Extent_{V_{i2}}$ is greater than e_{i2} and $VBRatio$ is more than r_i are saved (V_{i2b}). VIF represents the final segmented vessels. These steps are summarized in Algorithm 1. Also Fig.1 gives an example of vessel segmentation. All of the parameters in Algorithm 1 are shown as follows: $a_{i1} = 100$; $a_{i2} = 1000$; $e_{i1} = 0.2$; $e_{i2} = 0.29$; $r_i = 3$.

For binary image V_{m0}, the process of vessel segmentation and parameters are similar as V_{i0}. At first, the 4-connected regions in V_{m0} are divided into three parts according to *Area* of each connected region: $V_{m1}(0 < Area_{V_{m0}} < a_{m1})$, $V_{m2}(a_{m1} \le Area_{V_{m0}} < a_{m2})$ and $V_{m3}(Area_{V_{m0}} \ge a_{m2})$. V_{m3} is preserved and V_{m1} is abandoned. Secondly, the connected regions in V_{m2} are divided into two parts according to *Extent* of each each connected region: $V_{me1}(Extent_{V_{m2}} < e_m)$ and $V_{me2}(Extent_{V_{m2}} >= e_m)$. V_{me1} is saved. Also the connected regions in V_{me2}: $V_{me2a}(VBRatio > r_m)$ and $V_{me2b}(VBRatio \le r_m \&\& VCRatio > c)$ are preserved. VMF represents the final segmented vessels. These steps are summarized in Algorithm 2. Also Fig.2 provides the same example of vessel segmentation. All of the parameters in Algorithm 2 are shown as follows: $a_{m1} = 30$; $a_{m2} = 1000$; $e_m = 0.25$; $r_m = 2.2$; $c = 2$.

3) Vessel Combination: It can be observed that the operation of obtaining *VIF* can effectively identify vessel pixels while the operation of obtaining *VMF* can classify nonvessel pixels effectively. Thus, in order to obtain a good segmentation result, vessel combination is performed as follows:
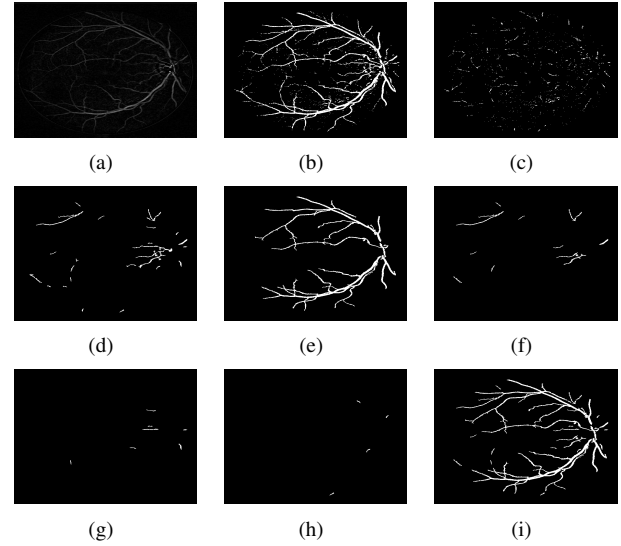

Fig. 2: Vessel segmentation after morphological reconstruction on an image from the DRIVE dataset. (a)Vessel enhanced image (T_{m0}). (b)Threshold image (V_{m0}). (c)$V_{m1}(0 < Area_{V_{m0}} < a_{m1})$. (d)$V_{m2}(a_{m1} \le Area_{V_{m0}} < a_{m2})$. (e)$V_{m3}(Area_{V_{m0}} \ge a_{m2})$ (f)$V_{me1}(Extent_{V_{m2}} < e_m)$. (g)$V_{me2a}(VBRatio > r_m)$. (h)$V_{me2b}(VBRatio \le r_m \&\& VCRatio > c)$. (i)The final segmented vessels (VMF).

Algorithm 2 : Vessel Segmentation After Morphological Reconstruction

Input:
Vessel Enhanced Image T_{m0}
Output:
The final segmented vessel image (VMF)
Process:

$$\forall(x,y), \quad V_{m0}(x,y) = \begin{cases} 1 & if\ T_{m0}(x,y) > p_m \\ 0 & otherwise \end{cases}$$

$$V_{m0} = \begin{cases} V_{m1} & if\ 0 < Area_{V_{m0}} < a_{m1} \\ V_{m2} & if\ a_{i1} \le Area_{V_{m0}} < a_{m2} \\ V_{m3} & if\ Area_{V_{m0}} \ge a_{m2} \end{cases}$$

$$V_{m2} = \begin{cases} V_{me1} & if\ Extent_{V_{m2}} < e_m \\ V_{me2} & if\ Extent_{V_{m2}} >= e_m \end{cases}$$

Let $a = [a1_{V_{me2}}, a2_{V_{me2}}, a3_{V_{me2}}, ..., an_{V_{me2}}]$ represent labels of each connected regions in V_{me2}

$$\forall x \in a \quad V_{me2a} = \begin{cases} 1 & if\ VBRatio_x > r_m \\ 0 & otherwise \end{cases}$$

$$V_{me2b} = \begin{cases} 1 & if\ VBRatio_x \le r_m\ \&\&\ VCRatio_x > c \\ 0 & otherwise \end{cases}$$

$$VMF = V_{m3} \cup V_{me1} \cup V_{me2a} \cup V_{me2b}$$

Firstly, the regions common to both *VIF* and *VMF* are extracted as the major vessels. For the remaining regions in *VMF*, we only abandoned the connected regions with $Area > 70\ \&\&\ Extent > 0.29\ \&\&\ VBRatio < 2.2$, resulting in vessel image V_{mf}. For the remaining regions in *VIF* (V_{IE}), the connected regions whose *Area* is less than a are saved (V_{IE1}). Next, skeleton extraction is performed to obtain the vessel skeleton of connected regions in V_{IE} whose *Area* is more than 70. Then SLIC is employed to generate superpixels [9] on vessel enhanced image (T_{i0}), which groups
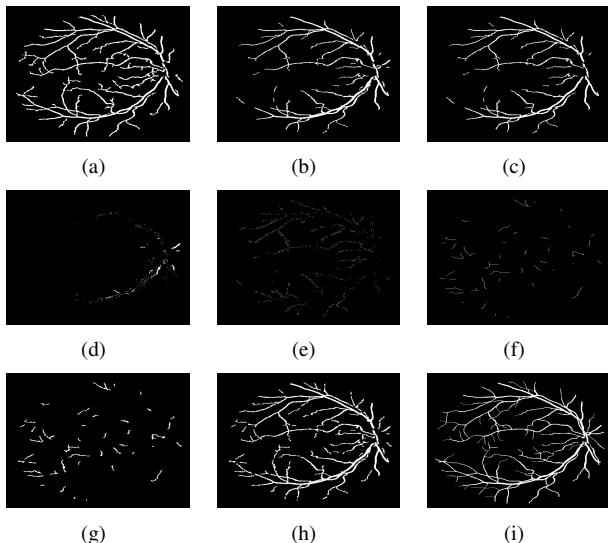
Fig. 3: Vessel combination. (a)Segmented vessel (VIF). (b)Segmented vessel (VMF). (c) The major vessels. (d)Vessel image V_{mf}. (e)Vessel image V_{IE1}. (f)Skeleton image in V_{IE}. (g)Skeleton expansion image. (h) Final vessel image after combination. (i) The ground-truth of this fundus image.

pixels into perceptually meaningful regions. Finally, skeleton expansion is implemented by means of a simple strategy that for each superpixel in T_{i0}, if it exists skeleton pixels, then this superpixel is considered as vessel superpixel and added to the final vessel image. The process of vessel combination is shown in Fig.3.

III. EXPERIMENTS AND RESULTS

In this section we present experiments to evaluate the performance of our proposed method. Three commonly used metrics were applied to evaluate the performance of the competing methods in terms of pixels: $Sensitivity(Se) = tp/(tp+fn)$, $Specificity(Sp) = tn/(tn + fp)$ and $Accuracy(Acc) = (tp + tn)/(tp + fp + tn + fn)$. tp, tn, fp and fn indicate the true positive (vessels), true negative (non-vessels), false positive (pixels falsely classified as vessels), and false negative (pixels falsely classified as non-vessels), respectively. Sensitivity is a ratio of well-classified vessel pixels. Specificity performs the same function for nonvessel pixels. Accuracy is a comprehensive measurement of pixels which can be classified correctly. Furthermore, the segmentation time of each image for implementing the proposed segmentation algorithm is recorded.

In order to show the effectiveness of the proposed method, we first compare our algorithm with other existing methods. Then the performance on the STARE Abnormal dataset is analyzed with the purpose of demonstrating the robustness of the proposed approach. For the DRIVE dataset and STARE dataset, the manual segmentations of the first observer are used as the ground truth. Because most existing methods have utilized the manual segmentations of the first observer to analyse the segmentation performance of blood vessels.

A. Vessel Segmentation Performance

The segmentation performance of blood vessels on the two test datasets is given in Table I. From Table I, it can be observed that the IUWT segmentation method and the morphological reconstruction method have good performance on segmentation accuracy. However, they have a low value of sensitivity or specificity. So the proposed method improves the segmentation performance by further combing two segmented vessel images *VIF* and *VMF* and produces a comprehensive good result.

In addition, Table II provides the results of the proposed algorithm and other methods. From Table II, it can be observed the proposed approach outperforms other existing methods in terms of accuracy except for [14]. However, the method [14] has high computational efficiency due to application of SVM classifier, which may need to train again for a new dataset. Also, from Table II, it can be observed that the sensitivity and specificity are competitive when compared with other methods.

B. Abnormal Image Analysis

TABLE III: THE PERFORMANCE OF VESSEL SEGMENTATION ON THE STARE ABNORMAL DATASET

Method	Acc	Time
Hoover *et.al.* [12]	0.9211	5min
Jiang *et.al.* [16]	0.9352	8-36s
Mendonca *et.al.* [17]	0.9426	3min
Soares *et.al.* [13]	0.9425	3min
Vermeer *et.al.* [24]	0.9287	-
Marin *et.al.* [1]	0.9510	90s
Lam and Yan [18]	0.9474	8min
Lam *et.al.* [7]	0.9556	13min
Roychowdhury and Koozekanani [15]	0.9453	8.36s
Roychowdhury *et.al.* [23]	0.9535	3.87s
Proposed	**0.9561**	**13.92s**

The existing algorithms [14], [17], [18] have demonstrated that the segmentation performance on abnormal retinal image can be applied to test the robustness of vessel segmentation algorithms. Table III gives the comparative segmentation performance of the proposed approach compared with other state-of-art methods on STARE Abnormal dataset. It can be observed that the proposed method outperforms all other methods in terms of accuracy and has low computational complexity on STARE Abnormal dataset, which demonstrates the robustness of the proposed algorithm.

IV. DISCUSSION AND CONCLUSION

The paper has proposed a novel and simple unsupervised vessel segmentation algorithm and evaluated it on two public datasets: DRIVE and STARE. This algorithm obtains two binary images by thresholding two vessel enhanced images, where one is enhanced by isotropic undecimated wavelet transform and another by morphological reconstruction. Then region features of blood vessels are used to extract initial segmented vessels. Finally, we combine two segmented vessel

TABLE I: THE SEGMENTATION PERFORMANCE OF THE PROPOSED METHOD ON THE TEST DATASETS

Dataset	Segmentation	Acc	Se	Sp	Time(s)
DRIVE Test	IUWT	0.9525(0.0047)	0.7542(0.0469)	0.9717(0.0072)	2.5151(0.1556)
	Morphological Reconstruction	0.9601(0.0048)	0.6604(0.0719)	0.9890(0.0047)	3.0883(0.4311)
	Proposed	0.9578(0.0038)	0.7408(0.0569)	0.9788(0.0063)	9.7080(0.7892)
STARE	IUWT	0.9516(0.0088)	0.8200(0.0700)	0.9621(0.0123)	4.4461(0.2663)
	Morphological Reconstruction	0.9578(0.0106)	0.7230(0.1913)	0.9763(0.0131)	3.6016(0.5113)
	Proposed	0.9580(0.0075)	0.7880(0.1268)	0.9716(0.0121)	14.5802(1.7566)
STARE Normal	IUWT	0.9501(0.0084)	0.8435(0.0690)	0.9584(0.0119)	4.4864(0.2581)
	Morphological Reconstruction	0.9638(0.0054)	0.8044(0.1454)	0.9756(0.0114)	3.8810(0.3440)
	Proposed	0.9600(0.0063)	0.8400(0.1083)	0.9689(0.0112)	15.2403(1.7185)
STARE Abnormal	IUWT	0.9530(0.0093)	0.7966(0.0660)	0.9659(0.0121)	4.4058(0.2819)
	Morphological Reconstruction	0.9517(0.0113)	0.6417(0.2034)	0.9770(0.0153)	3.3223(0.5101)
	Proposed	0.9561(0.0084)	0.7360(0.1274)	0.9743(0.0129)	13.9200(1.6101)

Mean performance metrics and their standard deviation is given in ().

TABLE II: COMPARATIVE PERFORMANCE OF THE PROPOSED METHOD ON THE TEST DATASETS WITH EXISTING METHODS

Test Data	DRIVE Test				STARE				
Method	Acc	Se	Sp	Time	Acc	Se	Sp	Time	System
Supervised	**Methods**								
Niemeijer *et.al.* [2]	0.942	0.689	0.969	-	-	-	-	-	-
Staal *et.al.* [11]	0.944	0.719	0.977	15min	0.952	0.697	0.981	15min	1.0 GH, 1 GB RAM
Soares *et.al.* [13]	0.946	0.733	0.978	∼3min	0.948	0.720	0.975	∼3min	2.17 GHz, 1 GB RAM
Ricci *et.al.* [14]	0.959	0.775	0.972	-	0.965	0.903	0.939	-	-
Marin *et.al.* [1]	0.945	0.706	0.980	∼90s	0.952	0.694	0.982	∼90s	2.13 GHz, 2 GB RAM
Fraz *et.al.* [3]	0.948	0.740	0.981	∼100s	0.953	0.755	0.976	∼100s	2.27 GHz, 4 GB RAM
Roychowdhury and Koozekanani [15]	0.952	0.725	0.983	3.11s	0.951	0.772	0.973	6.7s	2.6 GHz, 2 GB RAM
Unsupervised	**Methods**								
Hoover *et.al.* [12]	-	-	-	-	0.928	0.65	0.810	5min	Sun SPARCstation 20
Jiang *et.al.* [16]	0.891	0.83	0.9	8-36s	0.901	0.857	0.900	8-36s	600MHz PC
Mendonca *et.al.* [17]	0.945	0.734	0.976	2.5min	0.944	0.699	0.973	3min	3.2 GHz, 980 MB RAM
Lam *et.al.* [18]	-	-	-	-	0.947	-	-	8min	1.83 GHz, 2 GB RAM
Al-Diri *et.al.* [19]	-	0.728	0.955	11min	-	0.752	0.968	-	1.2 GHz
Lam and Yan [7]	0.947	-	-	13min	0.957	-	-	13min	1.83 GHz, 2 GB RAM
Budai *et.al.* [20]	0.949	0.759	0.968	11s	0.938	0.651	0.975	16s	2.0 GHz, 2 GB SDRAM
Budai *et.al.* [21]	0.957	0.644	0.987	-	0.938	0.58	0.982	-	2.3 GHz, 4 GB RAM
Perez *et.al.* [22]	0.925	0.644	0.967	∼2min	0.926	0.769	0.944	∼2min	Parallel Cluster
Miri *et.al.* [6]	0.943	0.715	0.976	∼50s	-	-	-	-	3 GHz, 1 GB RAM
Nguyen *et.al.* [5]	0.941	-	-	2.5s	0.932	-	-	2.5s	2.4 GHz, 2 GB RAM
Roychowdhury *et.al.* [23]	0.949	0.739	0.978	2.45s	0.956	0.732	0.984	3.95s	2.6GHz, 2 GB RAM
Proposed	**0.958**	**0.741**	**0.979**	**9.7s**	**0.958**	**0.788**	**0.972**	**14.6s**	**2.5 GHz, 8-GB RAM**

images with skeleton extraction and simple linear iterative clustering.

The proposed vessel segmentation performs well on abnormal retinal images since the algorithm use the region information of vessels. It achieves a vessel segmentation accuracy of 95.8% and 95.8% on images from two public datasets DRIVE and STARE, respectively. Our method outperforms other existing approaches except for the method of [14]. However, in [14], the computational time is much complex.

From above description, the proposed vessel segmentation algorithm has high computational efficiency and is independent on the training data. It is suitable for vessel pathology detection and analysis.

REFERENCES

[1] D. Marín, A. Aquino, M. E. Gegúndez-Arias, and J. M. Bravo, "A new supervised method for blood vessel segmentation in retinal images by using gray-level and moment invariants-based features," *IEEE Transactions on Medical Imaging*, vol. 30, no. 1, pp. 146–158, 2011.

[2] M. Niemeijer, J. Staal, B. van Ginneken, M. Loog, and M. D. Abramoff, "Comparative study of retinal vessel segmentation methods on a new publicly available database," in *Medical Imaging 2004*. International Society for Optics and Photonics, 2004, pp. 648–656.

[3] M. M. Fraz, P. Remagnino, A. Hoppe, B. Uyyanonvara, A. R. Rudnicka, C. G. Owen, and S. A. Barman, "An ensemble classification-based approach applied to retinal blood vessel segmentation," *IEEE Transactions on Biomedical Engineering*, vol. 59, no. 9, pp. 2538–2548, 2012.

[4] C. A. Lupascu, D. Tegolo, and E. Trucco, "Fabc: retinal vessel segmentation using adaboost," *IEEE Transactions on Information Technology in Biomedicine*, vol. 14, no. 5, pp. 1267–1274, 2010.

[5] U. T. Nguyen, A. Bhuiyan, L. A. Park, and K. Ramamohanarao, "An effective retinal blood vessel segmentation method using multi-scale line detection," *Pattern recognition*, vol. 46, no. 3, pp. 703–715, 2013.

[6] M. S. Miri and A. Mahloojifar, "Retinal image analysis using curvelet transform and multistructure elements morphology by reconstruction," *IEEE Transactions on Biomedical Engineering*, vol. 58, no. 5, pp. 1183–1192, 2011.

[7] B. S. Lam, Y. Gao, and A. W.-C. Liew, "General retinal vessel segmentation using regularization-based multiconcavity modeling," *IEEE Transactions on Medical Imaging*, vol. 29, no. 7, pp. 1369–1381, 2010.

[8] R. M. Haralock and L. G. Shapiro, *Computer and Robot Vision*. Addison-Wesley Longman Publishing Co., Inc., 1992.

[9] R. Achanta, A. Shaji, K. Smith, A. Lucchi, P. Fua, and S. Süsstrunk, "Slic superpixels compared to state-of-the-art superpixel methods," *IEEE Transactions on Pattern Analysis and Machine Intelligence*, vol. 34, no. 11, pp. 2274–2282, 2012.

[10] P. Bankhead, C. N. Scholfield, J. G. McGeown, and T. M. Curtis, "Fast retinal vessel detection and measurement using wavelets and edge location refinement," *PloS one*, vol. 7, no. 3, p. e32435, 2012.

[11] J. Staal, M. D. Abràmoff, M. Niemeijer, M. A. Viergever, and B. van Ginneken, "Ridge-based vessel segmentation in color images of the retina," *IEEE Transactions on Medical Imaging*, vol. 23, no. 4, pp. 501–509, 2004.

[12] A. Hoover, V. Kouznetsova, and M. Goldbaum, "Locating blood vessels in retinal images by piecewise threshold probing of a matched filter response," *IEEE Transactions on Medical Imaging*, vol. 19, no. 3, pp. 203–210, 2000.

[13] J. V. Soares, J. J. Leandro, R. M. Cesar, H. F. Jelinek, and M. J. Cree, "Retinal vessel segmentation using the 2-d gabor wavelet and supervised classification," *IEEE Transactions on Medical Imaging*, vol. 25, no. 9, pp. 1214–1222, 2006.

[14] E. Ricci and R. Perfetti, "Retinal blood vessel segmentation using line operators and support vector classification," *IEEE Transactions on Medical Imaging*, vol. 26, no. 10, pp. 1357–1365, 2007.

[15] S. Roychowdhury, D. D. Koozekanani, and K. K. Parhi, "Blood vessel segmentation of fundus images by major vessel extraction and subimage classification," *IEEE Journal of Biomedical and Health Informatics*, vol. 19, no. 3, pp. 1118–1128, 2015.

[16] X. Jiang and D. Mojon, "Adaptive local thresholding by verification-based multithreshold probing with application to vessel detection in retinal images," *IEEE Transactions on Pattern Analysis and Machine Intelligence*, vol. 25, no. 1, pp. 131–137, 2003.

[17] A. M. Mendonca and A. Campilho, "Segmentation of retinal blood vessels by combining the detection of centerlines and morphological reconstruction," *IEEE Transactions on Medical Imaging*, vol. 25, no. 9, pp. 1200–1213, 2006.

[18] B. S. Y. Lam and H. Yan, "A novel vessel segmentation algorithm for pathological retina images based on the divergence of vector fields," *IEEE Transactions on Medical Imaging*, vol. 27, no. 2, pp. 237–246, 2008.

[19] B. Al-Diri, A. Hunter, and D. Steel, "An active contour model for segmenting and measuring retinal vessels," *IEEE Transactions on Medical Imaging*, vol. 28, no. 9, pp. 1488–1497, 2009.

[20] A. Budai, G. Michelson, and J. Hornegger, "Multiscale blood vessel segmentation in retinal fundus images." in *Bildverarbeitung für die Medizin*, 2010, pp. 261–265.

[21] A. Budai, R. Bock, A. Maier, J. Hornegger, and G. Michelson, "Robust vessel segmentation in fundus images," *IEEE Journal of Biomedical Imaging*, vol. 2013, 2013.

[22] M. A. Palomera-Pérez, M. E. Martinez-Perez, H. Benítez-Pérez, and J. L. Ortega-Arjona, "Parallel multiscale feature extraction and region growing: application in retinal blood vessel detection," *IEEE Transactions on Information Technology in Biomedicine*, vol. 14, no. 2, pp. 500–506, 2010.

[23] S. Roychowdhury, D. D. Koozekanani, and K. K. Parhi, "Iterative vessel segmentation of fundus images," *IEEE Transactions on Biomedical Engineering*, vol. 62, no. 7, pp. 1738–1749, 2015.

[24] K. A. Vermeer, F. M. Vos, H. Lemij, and A. M. Vossepoel, "A model based method for retinal blood vessel detection," *Computers in Biology and Medicine*, vol. 34, no. 3, pp. 209–219, 2004.